Received: 28 June 2021 | Revised: 29 September 2021 | Accepted: 1 October 2021

DOI: 10.1002/ese3.993

Energy Science & Engineering
Open Access

ORIGINAL ARTICLE

Performance Comparison of single-slope solar still loaded with various nanofluids

G. S. Dhindsa[1] | **Vijay Kumar**[2] | **M. K. Mittal**[2] | **G.S. Sokhal**[1] | **Nima Khalilpoor**[3] | **Mohsen Sharifpur**[4,5] | **Alibek Issakhov**[6] | **Ravinder Tonk**[1]

[1]Department of Mechanical Engineering, Chandigarh University, Mohali, India

[2]Mechanical Engineering Department, Thapar Institute of Engineering & Technology, Patiala, India

[3]Department of Energy Engineering, Graduate School of the Environment and Energy, Science and Research Branch, Islamic Azad University, Tehran, Iran

[4]Department of Mechanical and Aeronautical Engineering, Clean Energy Research Group, University of Pretoria, Hatfield, Pretoria, South Africa

[5]Department of Medical Research, China Medical University Hospital, China Medical University, Taichung, Taiwan

[6]Faculty of Mechanics and Mathematics, Department of Mathematical and Computer Modelling, Al-Farabi Kazakh National University, Almaty, Kazakhstan

Correspondence
G. S. Dhindsa, Department of Mechanical Engineering, Chandigarh University, Mohali, Punjab- 140413, India.
Email: guridhindsa@yahoo.com

Nima Khalilpoor, Department of Energy Engineering, Graduate School of the Environment and Energy, Science and Research Branch, Islamic Azad University, Tehran, Iran.
Email: nimakhalilpoor@gmail.com

Mohsen Sharifpur, Clean Energy Research Group, Department of Mechanical and Aeronautical Engineering, University of Pretoria, Hatfield, Pretoria, South Africa.
Email: mohsen.Sharifpur@up.ac.za

Abstract

Nanofluids are great heat transfer carriers for collecting thermal energy in solar thermal applications. In the present study, a theoretical study of single-slope solar still (passive type) has been carried out by incorporating CuO, Al_2O_3, Ag, Fe_2O_3, and SiC-water nanofluids at different volume concentrations (0.02, 0.05, 0.08, 0.12, and 0.2). This analysis has been carried out with an optimum water depth of 0.02m as obtained from the experimental and theoretical studies. In order to validate the model, the experiments were conducted on solar still and then performance of still was compared. The analytical expression of the characteristic equation using Runga-Kutta ODE, for passive single slope solar still was found to be in good agreement with experiments carried out in Patiala, India. The total deviation for both experimental and theoretical distillate output of a still for a day was found to be 12.24%. Daily production for Al_2O_3-water-based nanofluid was found to be (14.22%) higher than simple solar still without nanofluid, followed by CuO (10.82%), Ag (8.11%), Fe_2O_3 (7.63%) and SiC (7.61%).

KEYWORDS

nanofluid, solar desalination, solar still, thermal model, thermo-physical properties

1 | INTRODUCTION

Earth, known as the mother of life, has a nectar-like fluid called water. Two-thirds of the earth's surface is covered with water, 97% of which is salty and the remaining is fit for drinking. The quality of drinkable water is deteriorating due to regress development and industrial setups; so, to improve its quality, different water purification methods are investigated and desalination of water with the help of solar still[1] was found to be the most efficient and clean way. The illustrative diagram of solar still is shown in Figure 1. Solar still operates on the principle of conversion of solar radiation into heat. First, the impure water is filled into the basin of the still. A tilted glass has been kept on the top of the still, through which the solar radiation is passed to the black absorber lining. The impure water in the basin absorbs the heat which gets evaporated and the pure water in the form of vapors is stuck on the surface of the glass and gets condensed. The condensed vapors get collected in a container through a distillate collection channel of the still.

Solar desalination systems are divided into two categories viz. passive solar stills and active solar stills. In the past few years, various researchers have studied the passive and active types of stills[2] and concluded that the performance of the passive type of still is better than that of the active type still. Dwivedi et al[3] investigate the performance of the double-slope passive-type solar still at three water levels. It was observed that in summers the performance of the double slope solar still was more, but the annual yield production of single slope solar still was higher than the double slope solar still. Xiao et al[4] reviewed the different types of solar stills and presented the fundamental heat and mass transfer process analysis, stated by Dunkle, Adhikari, Kumar, Elsafty, Tanaka, and Zheng. They have also integrated the solar reflectors in their studies and found the better performance of still for the regions having low solar incidence. Tiwari et al[5] analyzed the effects of orientation of still and glass cover inclination for the maximum yield both in summers and winters. Nafey et al[6] used a floating wick system in experiments and found some major enhancements in the productivity of still. Singh et al[7] studied the effects of some parameters like glass cover material, environmental conditions, insolation per day, the orientation of the still, wind speed, and inclination of the glass cover. Aboul-Enein[8] investigated the effect of water depth, the inclination of the glass cover, and optimum insulation for the still. Samee et al[9] studied various design parameters of single basin solar still and observed an optimum cover glass inclination and glass thickness of around 33.3° and 3 mm both in summer and winters for the southwest arid region. Abu-Hijleh et al[10] performed some experiments having water film cooling on the glass cover and the efficiency of the film cooling still was found to be non-sensitive to the wind speeds. Tiwari and Anil[11] analyzed the seasonal variation of distillate output at different water depths. Dunkle et al[12] correlate both convective heat transfer coefficient and evaporative heat transfer coefficient with experimental validation and it was found to be in good agreement of about 2% of the variation. Kumar et al[13] presented the annual performance of active solar still for the location in New Delhi. Singh et al[6] proposed an experimental and theoretical model of double slope solar still with an inclination angle of 55°.

Sakthovel et al[14] observed and proposed a mathematical model integrating jute cloth in the water medium, which maximizes the surface area of water and helps in getting more evaporation rates. Srivastava et al[15] proposed an experimental setup with multiple porous floating absorbers and studied its performance. Aboul et al[8] investigated the effects of deep basin-type solar stills. El-Bahi et al[16] experimented with double glass solar still and integrated a

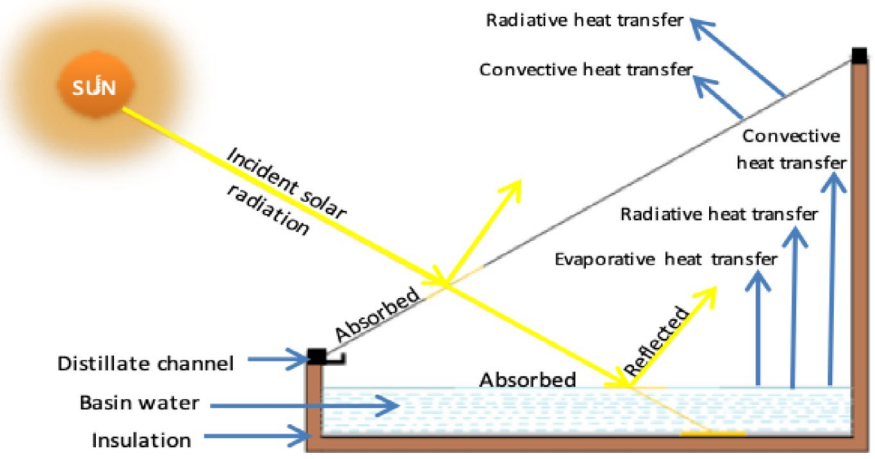

FIGURE 1 Simple solar still

separate condenser. Abu-Arabi et al[17] investigated double-glass cover solar still with an added cooling effect on the glass and observed that the efficiency for the still having perfect airtight insulation was more as compared to the double glass. Nafey et al[6] developed a thermal model to estimate the distillate output of the still having floating balls and a thin sheet of black color. El-Sebaii[18] worked with a suspended absorber which divides the water into two halves that increase daily productivity by (18.5%-20%). Al-Hussaini et al[19] created a vacuum inside the solar still and observed an increase in more than 100% because of zero convective heat transfer coefficient and increase in evaporative heat transfer coefficient. Sodha et al[20] worked with a multi-wick system and observed an increase of 42% in comparison with simple solar still.

The seeding nanoparticles in base fluid enhance the heat transfer coefficients and result in better performance of still. Several authors have done thermal modeling of nanofluids to find their properties and performance for various applications.[21-28] Sahota et al[29] investigated the performance of three different nanoparticles (Al_2O_3, TiO_2, CuO) at different volume concentrations (0.01, 0.093, 0.131) and observed an increase in convective heat transfer coefficient by 67.03%, 63.56%, and 71.23%, also he observed an increase in Nuscelt number by 119.72%, 98.64%, and 151.62%. Sahota et al[30] observed a decrease in entropy generation when CuO nanoparticle is used, and he observed a performance trend of $CuO > TiO_2 > Al_2O_3 > SiO_2$. Omid et al[31] observed peak absorption characteristics of nanoparticles on a particular wavelength, with the change in diametrical size resonance nature changes. Omara et al[32] used solar still having both nanofluid and corrugated wick and maintained vacuum inside the still, to minimize the convective heat transfer. Sharshir et al[33] investigated simple solar still with nanoparticles and glass cover cooling and experienced a productivity increase of 44.91% and 53.95%. Rashidi et al[34] investigated a CFD analysis with stepped solar still integrated with nanofluids and found a 2.1% variation between his experimental and simulated work. Chen et al[35] reviewed the optical and thermal properties of nanofluid and observed that SiC nanoparticles have a good effect for enhancing both thermal (6% increase with 0.4% volume fraction) and transport properties. Kabeel et al[36] worked with an absorber plate coated with the black nanoparticle. Liu et al[37] performed an experiment on a solar collector integrated with nanoparticles and observed a constant 10°C rise in the temperature of nanofluid with distilled water. Abujazar et al[38] worked with inclined stepped solar still with copper trays and found higher performance due to the higher conductivity of copper. Elashmawy et al[39] used a parabolic concentrator solar tracking system integrated with a simple solar still. It enhanced the performance of the solar still by 676%. Sahota et al[40] experimented on passive double slope solar still with water-based nanofluid ($Al2O_3$, TiO_2, and CuO) and observed an increase in (19.1%, 10.38%, 5.25%) in terms of productivity. Kabeel et al[41] used graphene oxide nanoparticles in the phase change material (PCM) to improve the thermal conductivity of nano-doped phase changed material by 52%. Tubular solar still loaded with PCM increases the water temperature by 7ºC and without phase change material it was found to be 3ºC. There was a 24% increase in temperature of nano-doped phase change materials as compared to phase change material without nanoparticles. Total yield for tubular solar still, tubular solar still with PCM, and tubular solar still with NPCM was found to be 2.59, 3.35, and 5.62 kg/m^2, respectively. Subhedar et al[42] performed an experiment in which a parabolic trough collector was integrated with conventional single-slope solar still. Water and Al_2O_3 nanofluid was taken as working fluid with 0.05% and 0.1% volume fraction, respectively. The rise in productivity and thermal efficiency was found to be 66% and 70% with the use of Al_2O_3 nanofluid in the complete integrated system.

The performance of the still depends upon some properties, like the volume fraction, particle size, and thermophysical properties like specific heat capacity, viscosity, and density. Nanoparticle generally is defined as the ratio of its surface area to the volume, if it is significant, then it is known as nanoscale material. This ratio increases the properties like thermal conductivity, thermal diffusivity, viscosity, electric conductance, and optical sensitivity changes.[7] Nanoparticles are tiny particles of size in the range of 1 to 100 nanometers (nm). As the particle size decreases, the transport and physical property of the particle change, which affects the performance of the still. Every nanoparticle size has a different wavelength at which it absorbs the maximum solar energy, which is known as resonant wavelength. So, the size of the nanoparticle is an important parameter.[7] Specific heat capacity of the fluid has a great effect on the performance of the solar still. When the solar radiation hits the surface, a portion of the sun's energy gets absorbed in sensible heating and the remaining goes into the latent heat storage. Thermal conductivity of the nanoparticle increases when the surface area to volume ratio increases, which means as size goes down, the performance of the solar still having nanofluid improves.[9] Using metallic nanoparticles of different sizes help solar still to capture all the incident range because of different resonant wavelength to each size.[7]

According to the coined literature review, limited research has been carried out on developing a thermal model on single-slope solar still having nanofluids, with a comparison of its effects at different volume concentrations. Therefore, the main purpose of the present research is to analytically investigate the effects of nanofluid at

different volume concentrations for various nanoparticles and validate it with the experimental result. Moreover, it can also help to fill the technological gap to compare the performance of solar still with different nanoparticles and their concentration.

2 | EXPERIMENTAL SETUP AND PROCEDURE

The simple single-slope solar still have been constructed, a basin was made of stainless steel-grade 304 in the shape of a rectangular tray having an evaporating surface area of 1 m^2. The glass cover was inclined at 30° with the horizontal surface, which is almost equal to the latitude of the location. The sides of the tray were insulated with glass wool, rubber-type material was used as basin liner of thickness 5 mm to absorb the maximum solar energy and to transmit that energy to basin water. A constant water level is maintained by a constant head device arrangement. A sponge rubber gasket is installed between the glass and the tray, which helps to ensure there are no gaps between the glass panels. The tray is insulated from the ambient conditions as shown in Figure 2. The system was oriented toward the south. Window glass was used as a condensation surface and transparent cover from where the incident radiation enters into the still. To avoid some drops of distillate falling back to the evaporator surface, a rectangular plastic cross-sectional channel is fixed to the bottom of the glass cover.

In addition to this K-type, thermocouples were used to measure the temperatures and a data logger was employed to log the temperature data. The ambient temperature was observed between 31 and 41°C. Pyranometer was used to measure the direct radiation and diffused radiations incident on the surface. It has been found that the solar radiation varied from 12 to 830 W/m^2. The wind velocity was varied from 0.1 to 2.5 m/s and was measured using the anemometer. The distillate was collected in a container at an interval of 1 hour and measured with a digital weighing pan.

3 | THERMAL MODELING

3.1 | Mathematical model

The mathematical model attempts to describe the energy transition at every step of the still. Figure 1 shows the energy transfer involved in the still.

3.2 | Energy balance

3.2.1 | Energy balance for basin liner

The solar energy falling on solar still was stored in the basin and remaining energy lost to the atmosphere through a convective heat transfer and energy balance can be written as:

$$\alpha_b \tau_g \tau_w I(t) A_b = m_b cp_b \frac{dT_b}{dt} + Q_{cb} + Q_w \tag{3.1}$$

where Q_{cb} convective heat transfer from basin liner to water, which can be calculated as

$$Q_{cb} = h_w A_b \left(T_b - T_w\right), \tag{3.2}$$

and, Q_W is the heat lost to ambient and can be calculated as

$$Q_w = h_b A_b \left(T_b - T_a\right) \tag{3.3}$$

T_b, T_a, T_w are the basin temperature, ambient temperature, and water temperature, respectively.

FIGURE 2 Experimental setup of single slope solar still

3.2.2 | The transition energy balance for water mass

The energy balance of water can be represented as:

$$Q_u + \alpha_w \tau_g I(t) A_w + Q_{cb} = m_w cp_w \frac{dT_w}{dt} + Q_{cw} + Q_{rw} + Q_{ew} \tag{3.4}$$

Q_u is the external heat supplied. For this passive type of still, the value of Q_u is zero and Q_{cw} is the convective heat transfer from the water to glass.[12]

$$Q_{cw} = 0.884\left(T_w - T_g + \frac{(P_w - P_g)(T_w + 273.15)}{(268900 - P_w)}\right) A_w (T_w - T_g) \tag{3.5}$$

where P_w and P_g are partial vapor pressure at the water and the glass cover and can be determined as[12]

$$P_w = \exp\left(25.317 - \frac{5144}{T_w + 273.15}\right) \tag{3.6}$$

$$P_g = \exp\left(25.317 - \frac{5144}{T_g + 273.15}\right) \tag{3.7}$$

Q_{rw} is the radiative heat transfer between water and glass, ε_{eff} is the effective emittance, and σ is the Stefan-Boltzman's constant and can be calculated as[12]

$$Q_{rw} = \sigma \varepsilon_{eff} A_w \left((T_w + 273.15)^4 - (T_g + 273.15)^4\right) \tag{3.8}$$

Q_{ew} is radiative heat transfer between water and glass and can be calculated as[12]

$$Q_{ew} = \frac{0.016237\left(h_{cw}(P_w - P_g)\right)}{(T_w - T_g)} A_w (T_w - T_g) \tag{3.9}$$

If it is a passive solar still, $Q_u = 0$ signifies the external heat transfer and it can be calculated as[10]

$$Q_u = A_c F_R (\propto \tau)_c I(t)' - U_L (T_w - T_a) \tag{3.10}$$

where, $I(t)'$ is the incident radiation on solar collector surface.

3.2.3 | Energy balance for glass cover

The energy balance of the glass cover can be represented by the following equation:

$$\alpha_g I(t) A_g + Q_{cw} + Q_{rw} + Q_{ew} = m_g cp_g \frac{dT_g}{dt} + Q_{rg} + Q_{cg} \tag{3.11}$$

Q_{cg} is the convective heat transfer between the glass to ambient, and V is the wind velocity[3]

$$Q_{cg} = (2.8 + 3V) A_g (T_g - T_a) \tag{3.12}$$

Q_{rg} is the radiative heat transfer between glass cover to the sky[3]

$$Q_{rg} = \sigma \varepsilon_g A_g \left(\frac{(T_g + 273.15)^4 - (T_{sky} + 273.15)^4}{(T_g - T_a)}\right)(T_g - T_a) \tag{3.13}$$

To find the hourly distillate of the still,

$$m_d = \frac{h_{ew}(T_w - T_g)}{LH} \times 3600 \tag{3.14}$$

where LH is the latent heat of vaporization and can be determined as[3]

$$LH = 2.4935 \times 10^6 \left(1 - 9.4779 \times 10^{-4} T_w + 1.3132 \times 10^{-7} T_w^2 - 4.7974 \times 10^{-9} T_w^3\right) \quad (If\ T_w < 70) \tag{3.15}$$

$$LH = 3.1615 \times 10^6 \left(1 - 7.616 \times 10^{-4} T_w\right) \quad (\text{If } T_w > 70) \tag{3.16}$$

On solving the energy balance Equations (3.1), (3.4), and (3.11), one can obtain the first-order differential equation to find the temperatures (T_w, T_g, T_b) after the time interval "Δt".[11]

$$\frac{dT_w}{dt} + aT_w = f(t) \tag{3.17}$$

$$\text{where} a = \frac{A_c F_R + U_{lb} A_b + U_{lg} A_b}{m_w c_w} \tag{3.18}$$

$$f(t) = \frac{A_c F_R (\alpha\tau)_c I'(t)}{m_w c_w} + \frac{\left(A_c F_R U_l + U_{lb} A_b + U_{lg} A_b\right) T_a}{m_w c_w} + \frac{\left(\alpha_g h' + \alpha_w \tau_g + \alpha_b \tau_g \tau_w h A_s I(t)\right)}{m_w c_w} \tag{3.19}$$

where Equation (3.17) can be written as

$$T_{w(i+1)} = \frac{f(t)}{a}\left[1 - \exp(-at)\right] + T_{w(i)} \exp(-at) \tag{3.20}$$

$T(w(i+1))$ is the water temperature after Δt time interval.

Mass of distillate m_{ew} can be determined by only knowing the heat transfer by evaporation and the latent heat

$$m_{ew} = (qew \times 3600)/LH \tag{3.21}$$

$$\text{where } q_{ew} = h_{ew} \times \left(T_w - T_{gi}\right) \tag{3.22}$$

$$\frac{dT_w}{dt} = \frac{T_{w(i+1)} - T_{w(i)}}{\Delta t} \tag{3.24}$$

where $T_{w(i)}$, is the temperature of water at $t = 0$, and $T_{w(i+1)}$ is the water temperature after Δt time.

Now, for temporal discretization, Equations (3.1), (3.4), and (3.11) can be written for the time step of 0.1 seconds as,

$$T_{w(i+1)} = \left(A_c F_R (\propto \tau)_c I(t)' + A_c F_R U_L T_a + \alpha_w \left(1-\alpha_g\right) A_w I(t) + h_{c,b-w} A_w T_b + h_{lw} A_w T_g - h_{c,b-w} A_w T_w - h_{lw} A_w T_w - A_c F_R U_L T_w + \frac{m_w c_w}{\Delta t} T_w\right) \frac{\Delta t}{m_w c_w} \tag{3.25}$$

$$T_{g(i+1)} = \left(\alpha_g A_g I(t) + h_{lw} A_w T_w + h_{lg} A_g T_a - h_{lw} A_w T_g - h_{lg} A_g T_g + \frac{m_g c_g}{\Delta t} T_g\right) \frac{\Delta t}{m_g c_g} \tag{3.26}$$

$$T_{b(i+1)} = \left(\alpha_b \left(1-\alpha_g\right)\left(1-\alpha_w\right) A_b I(t) + h_{c,b-w} A_b T_w + h_b A_b T_a - h_{c,b-w} A_b T_b - h_b A_b T_b + \frac{m_b c_b}{\Delta t} T_b\right) \frac{\Delta t}{m_b c_b} \tag{3.27}$$

The efficiency of the still is defined as the ratio of the useful energy output to the total energy incident on the surface. The useful energy is defined as the product of distillate output to the latent heat absorbed by it.

$$\eta_{still} = \left(\frac{m_{ew} \times LH}{A_s \times I(t)}\right) \times 100 \tag{3.23}$$

where I is the solar incident radiation for t time.

Assumptions taken during the simulation

1. No vapor leakage from the still.
2. The heat capacity of the still has been neglected.
3. There is no temperature gradient along the glass cover thickness.
4. Each component of the system is perfectly insulated including pipes.
5. The solar distiller unit is vapor-leakage proof and is quasi-steady state.

3.3 | Validation theories

3.3.1 | Temporal discretization with a time step of 0.1 sec

A mathematical technique is adopted for transient conditions that happen to be the field of applied physics and mathematics; here, transient equations are being solved by discretizing time. Backward differencing for the first-order equation is used which is stated as

So, by knowing the initial temperatures T_w, T_g, T_b, and T_a, I(t) for every time interval Δt, we can estimate $T_{w(i+1)}$, $T_{g(i+1)}$,$T_{b(i+1)}$ and further mass of distillate.

3.3.2 | Numerical Iterative method

This model is based on Runga-Kutta (ODE) method for an iterative solution using the functions given by Kumar and Tiwari.[11] With the time step of 0.1 seconds, data for 24 hours is being simulated. Equations (3.1), (3.4), and (3.11) are used which is the $f(Tg, Tw, Ta, Tb, I(t), t)$.

$$T_w(i+1) = T_w(i) + (1/6)(k1tw + (2 \times k2tw) + (2 \times k3tw) + k4tw) \times t \tag{3.28}$$

$$T_g(i+1) = T_g(i) + (1/6)(k1tw + (2 \times k2tg) + (2 \times k3tg) + k4tg) \times t \tag{3.29}$$

$$T_b(i+1) = T_b(i) + (1/6)(k1tb + (2 \times k2tb) + (2 \times k3tb) + k4tb) \times t \tag{3.30}$$

where

$$k1tw = hf\left(T_w, T_g, T_b, T_a, I(t), t\right) \tag{3.31}$$

$$k1tg = hf\left(T_w, T_g, T_b, T_a, I(t), t\right) \tag{3.32}$$

$$k1tb = hf\left(T_w, T_g, T_b, T_a, I(t), t\right) \tag{3.33}$$

$$k2tw = hf(T_w + \frac{k1tw}{2}, T_g + \frac{k1tg}{2}, T_b + \frac{k1tb}{2}, T_a, I(t), t + \frac{h}{2}) k2tg = hf(T_w + \frac{k1tw}{2}, T_g + \frac{k1tg}{2}, T_b + \frac{k1tb}{2}, T_a, I(t), t + \frac{h}{2}) k2tb = hf(T_w + \frac{k1tw}{2}, T_g + \frac{k1tg}{2}, T_b + \frac{k1tb}{2}, T_a, I(t)$$

In order to validate with accuracy of the mathematical model, the experiment was conducted on solar still on 14 July 2019.

4 | METHODOLOGY

An experiment is carried out on single-glass solar still on 14th July 2019 at Patiala, India. The water level in the still is maintained at 3 cm. The thermal model is being validated with the corresponding results obtained by the experiment.

The flow chart of thermal modeling done using MATLAB software is shown in Figure 3. Initially, the temperature values of T_w, T_g, and T_b were taken equal to the ambient temperature. Further, the metalogical data measured using various instruments have been taken and loaded to compute heat transfer coefficients. The energy balance equations were then solved for glass cover, water, and basin liner. After this, the next iteration of temperatures of T_w, T_g, and T_b have been calculated. Finally, the distillate output has been calculated, and then the program stopped. During the simulation, first, the temporal discretization is being carried out, which is a FEM (finite element method) technique, to get a minimum deviation from the results. Runga-Kutta method is employed with the time step of 0.1 seconds, which generates a lower scope of error because of the closeness in the ambient temperature and intensities for the time gap. The perimeters of both the experimental model and thermal model are then compared for the hourly variation of distillate output and heat transfer coefficients.

After validation, the same thermal model is extended to determine the performance while using nanoparticles at different volume fractions. This model is carried out with an assumption that the value of ambient temperature and solar intensity falling on the surface is not changing for Δt time.

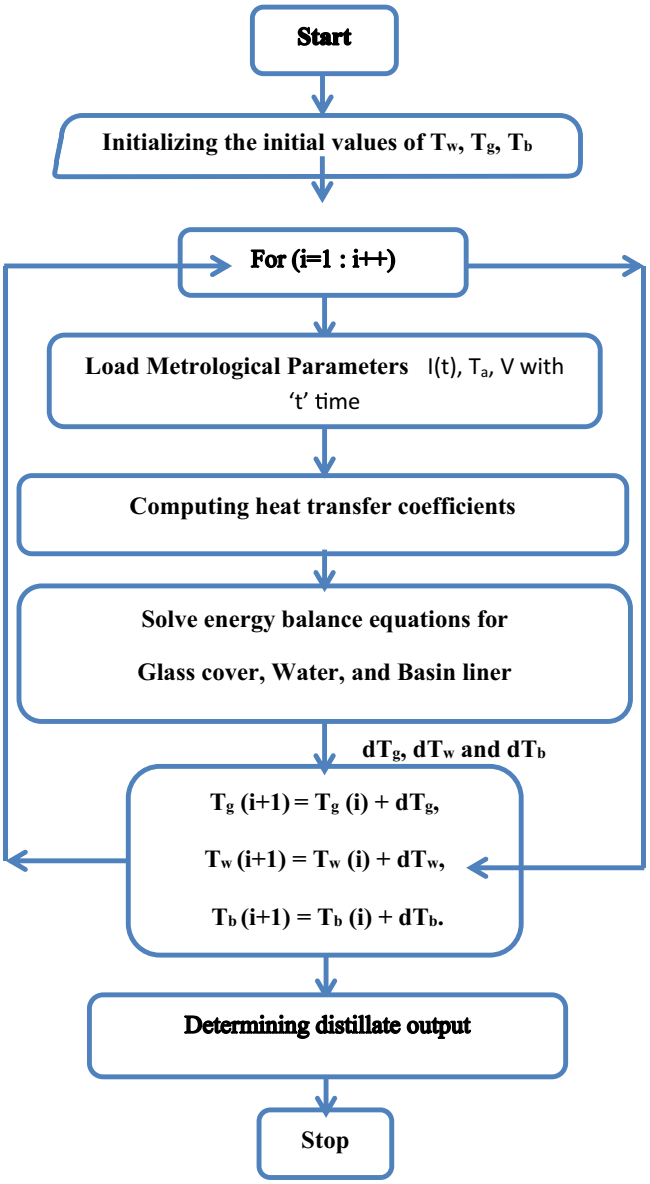

FIGURE 3 Flowchart of thermal modeling

5 | RESULTS AND DISCUSSIONS

An experiment was performed on a single-slope solar still (passive type) with a water depth of 0.03 m and glass tilt angle of 30° on 14 July 2019, the total distillate output obtained was 3.327 kg/(day.m^2). The hourly variation in solar intensity and ambient temperature with respect to time are shown in Figures 4 and 5, it can be seen from the graphs that the solar intensity and ambient temperature are maximum around 12:00 PM–01:00 PM, respectively. The maximum value of solar intensity was 830 W/m^2 and for ambient temperature was 41°C.

In the present study, the hourly experimental and theoretical observations were compared. The various design parameters of solar still are presented in Table 1. The inclination of the glass cover was kept at 30°C, which is equivalent to the latitude of the equation. The

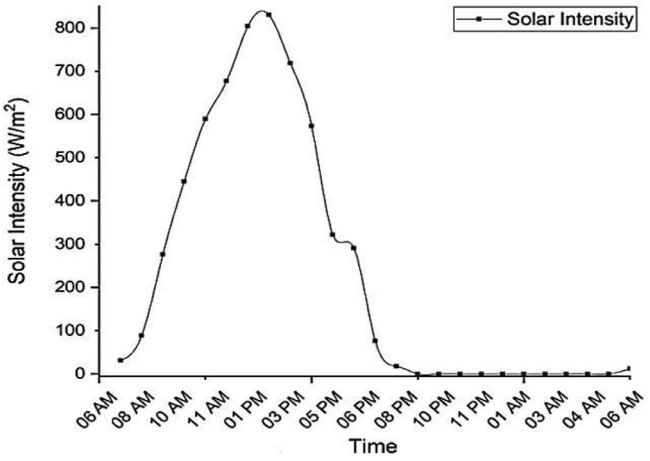

FIGURE 4 Variation of solar intensity on 14 July

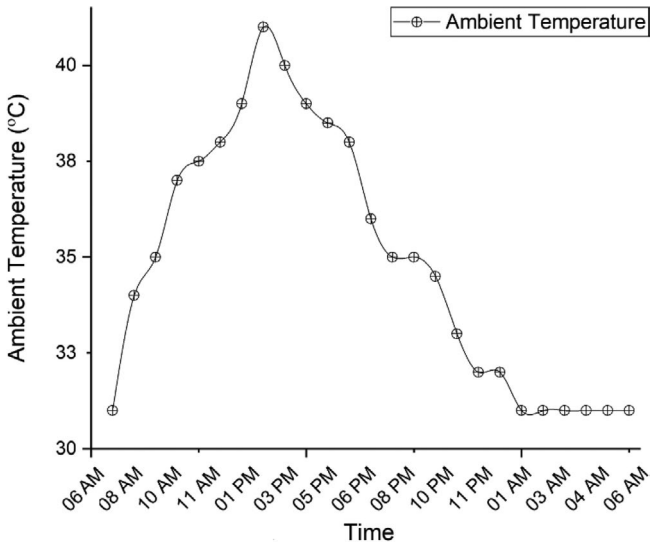

FIGURE 5 Variation of ambient temperature on 14th July

TABLE 1 Various design parameters of solar still

A_b	1 m^2	r_w	0.05
A_s	1 m^2	r_g	0.05
A_g	$A_b/\cos(\beta_s)$ m^2	τ_g	0.9
C_w	4190 (J/kgK)	ul	8
C_g	753 (J/kgK)	ξ_w	0.95
C_b	460 (J/kgK)	ξ_g	0.94
ρ_g	1500 (kg/m^3)	V	1 m/s
α_w	$1-\tau_w-r_w$	α_b	0.95
Water depth	0.03 m	α_g	0.05
Glass angle	30°		

basin and surface area of basin water was kept at 1 m^2. While the glass area can be calculated using the geometry of solar still as mentioned in Table 1. The basin of still was designed to store water up to the depth of 0.03 m. The convective heat transfer coefficients and optical properties of solar still components are also mentioned in Table 1.

5.1 | Validation of Thermal model

Theoretical model (using Runga-Kutta ODE integrated with a analytical model by Tiwari[11]) has been developed and compared with the experimentally obtained results. The predicted values of water temperature and glass temperature were in an average deviation range between 8% and 6% as shown in Figures 6 and 7. Figure 6 represents the hourly variation of theoretical and experimental water temperature and it has been observed a similar trend for both cases. The temperature of water starts rising as the solar intensity increased and tend to decrease during the later part of the day along with the solar intensity.

While Figure 7 represents the variation of glass temperature for 24 hours and it has been observed that variation in glass temperature of experimental and theoretical was more during the early part of the day. It is because the losses that occurred in actual condition were more than the theoretical loss considerations. From Figures 6 and 7, it has been observed that at the higher temperature, the ranges deviation from the experimental results are significant and it was because of the fact that the

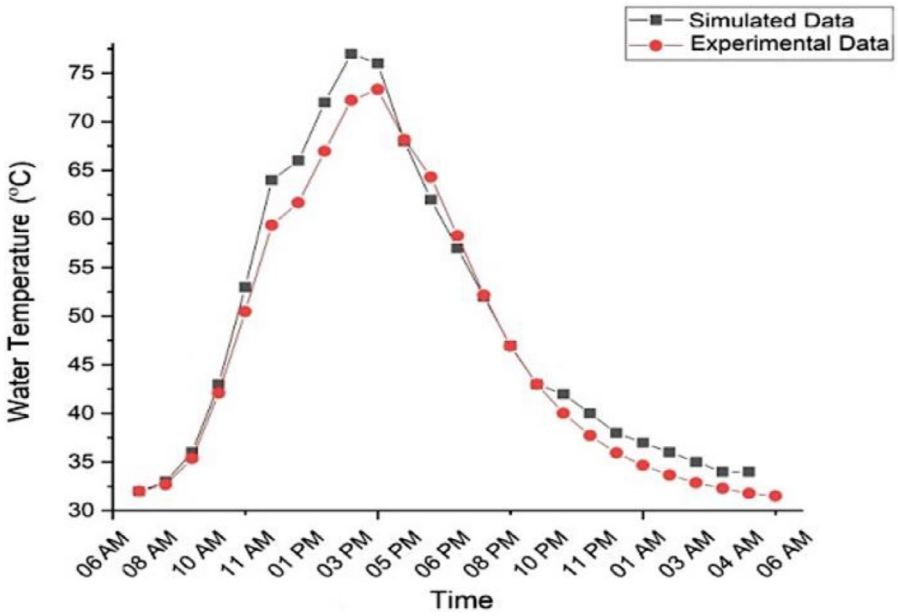

FIGURE 6 Hourly variation of theoretical and experimental water temperature

heat losses from the side insulations were more at higher temperatures.

The hourly variation of theoretical and experimental distillate output is shown in Figure 8. The productivity still follows the same trend as followed by the solar intensity. The experimental results are in good agreement with theoretical with a total deviation of 12.24% for both experimental and theoretical distillate output for a day and at higher temperatures, the range of deviation was found to be more. It is because of more losses from the still at higher temperature and solar intensity.

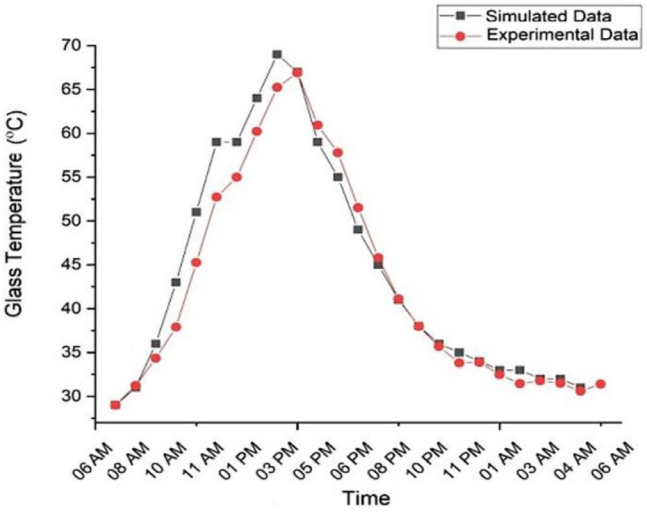

FIGURE 7 Hourly variation of theoretical and experimental glass temperature

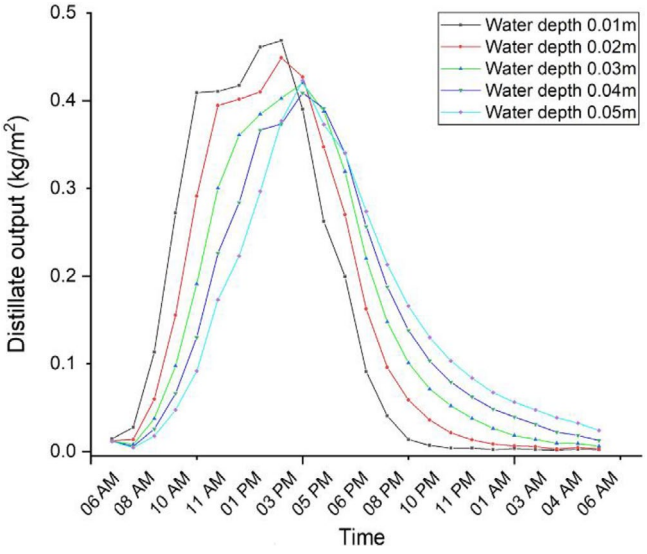

FIGURE 9 Hourly variation of distillate output at different water depths

5.2 | Effect of water depth on the performance of solar still

To obtain optimum water level, a mathematical simulation was carried at different water depths (0.01, 0.02, 0.03, 0.04, 0.05 m). As illustrated in Figure 9, at 0.01 m water depth, there exists a maximum peak value for distillate produced during the time 12:00 PM– 2:00 PM. As water depth increases, the graph shifts toward the right-hand side, which is because of the heat-storing capacity

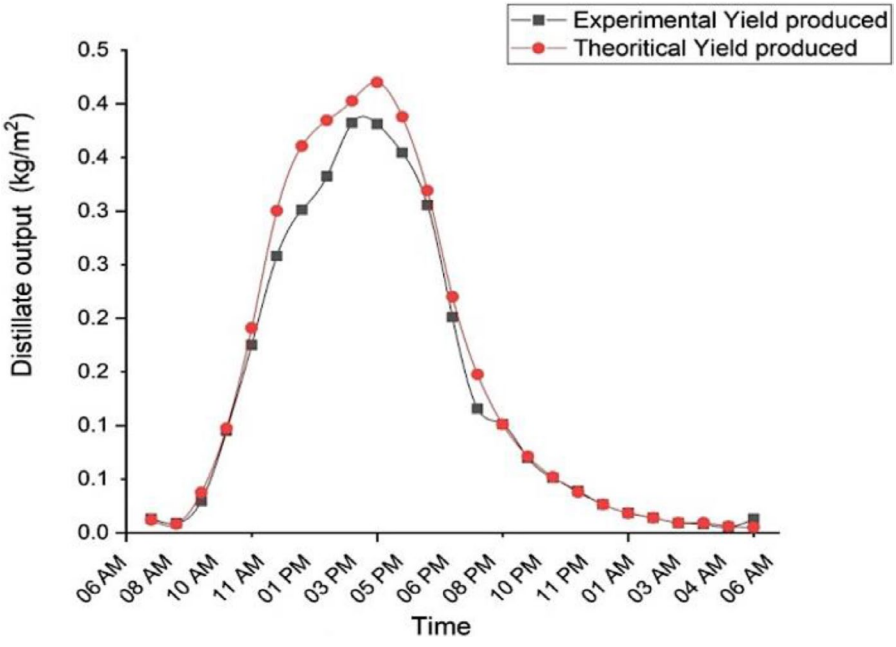

FIGURE 8 Hourly variation of theoretical and experimental distillate output

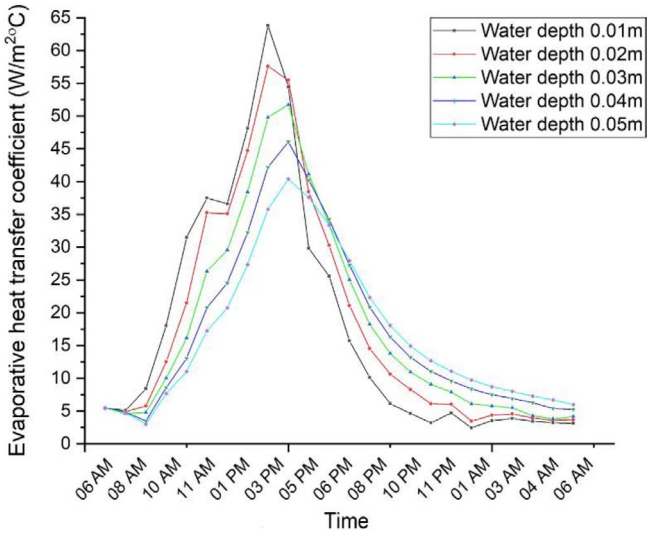

FIGURE 10 Hourly variation in evaporative heat transfer coefficients at different water depths

TABLE 2 Properties of nanoparticles

Material	'ρ' (kg/m^3)	'K' (W/mK)	'C_p' (J/K)
SiC	3160	490	675
Al_2O_3	3880	36	773
CuO	6350	69	535
Fe_3O_4	5180	6	670
Ag	10 490	0.235	429

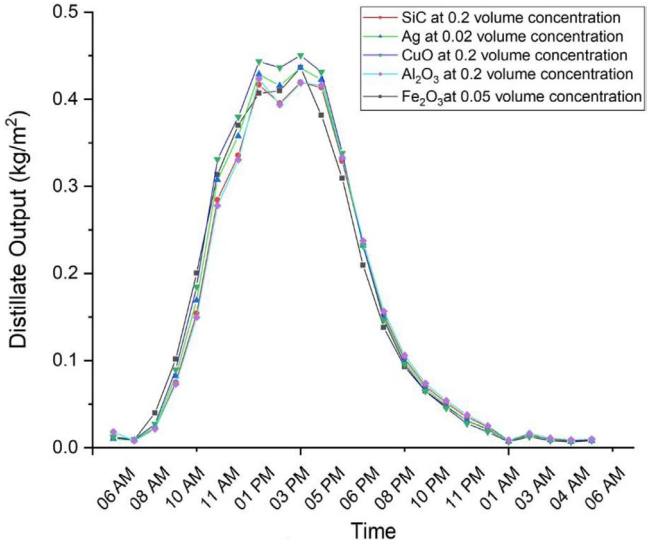

FIGURE 11 Hourly variation of distillate output for different nanofluids

of water. The maximum distillate output was recorded for 0.02 m with 3.65 kg/(day.m^2) and minimum for 0.08 m with 3.10 kg/(day.m^2). As the depth of the basin water increased, the day distillate decreased but night distillate increased because heat storage takes place in the basin water at more basin water depth.

Figure 10 shows the variations of evaporative heat transfer coefficients at various depths of basin water and a similar trend has been found as of hourly distillate output. The evaporative heat transfer coefficient for different water depths is maximum for the water level at 0.01 m having a peak during 2:00 PM, followed by 0.02 m and so on. The increasing trend of evaporative heat transfer slightly decreases at about noon at all depths of basin water because the solar intensity is almost at peak and temperature difference decreased.

5.3 | Variation in the performance of solar still with different Nanofluids

Seeding nanoparticles in the base fluid enhances heat transfer coefficients and results in higher performances. Also, increasing the volume fraction of the nanoparticle, the effective medium (surface area to volume ratio) increases, which contributes to higher efficiencies due to an increase in surface area.

Exceeding optimum levels of concentrations, there exists a noticeable change in flow resisting properties (with an increase in mass concentrations, the flow friction increases), and as a result, the viscosity increases. Increasing viscosity decreases the heat transfer efficiency.[40] With the maximum distillate output of 3.65 kg/(day.m^2) by simple solar still, 0.02 m was found to be the optimum water level to continue mathematical simulation for modified solar still, seeded with nanofluids.

The thermophysical behavior of a nanofluid depends on the particle size, volume fraction, and physical characteristics like density, thermal conductivity, and specific heat capacity. Also, the properties of nanoparticles are presented in Table 2. Figure 11 shows the distillate output for five different water-based nanofluids (CuO, Al_2O_3, SiC, Fe_2O_3, and Ag) that were simulated in MATLAB using Runga-Kutta numerical integration method. A higher yield of still was obtained for Al_2O_3 nanofluid with a 14.22% increase in productivity at a volume fraction of 0.2 as compared to water. While the enhancement of productivity with CuO, Ag, Fe_2O_3, and SiC at 0.2 volume fraction was found to be 10.82%, 8.11%, 7.63%, and 7.61%, respectively.

From simulation results, the temperature of nanofluid and base fluid (water) has been calculated and the differences of these temperatures have been taken. The temperature gradient for Al_2O_3 nanofluid was maximum because of the improved thermo-physical properties, as compared to the other simulated nanofluids. From Figure 12, it has been noticed that the peak temperatures for all the nanofluid were during the sunshine

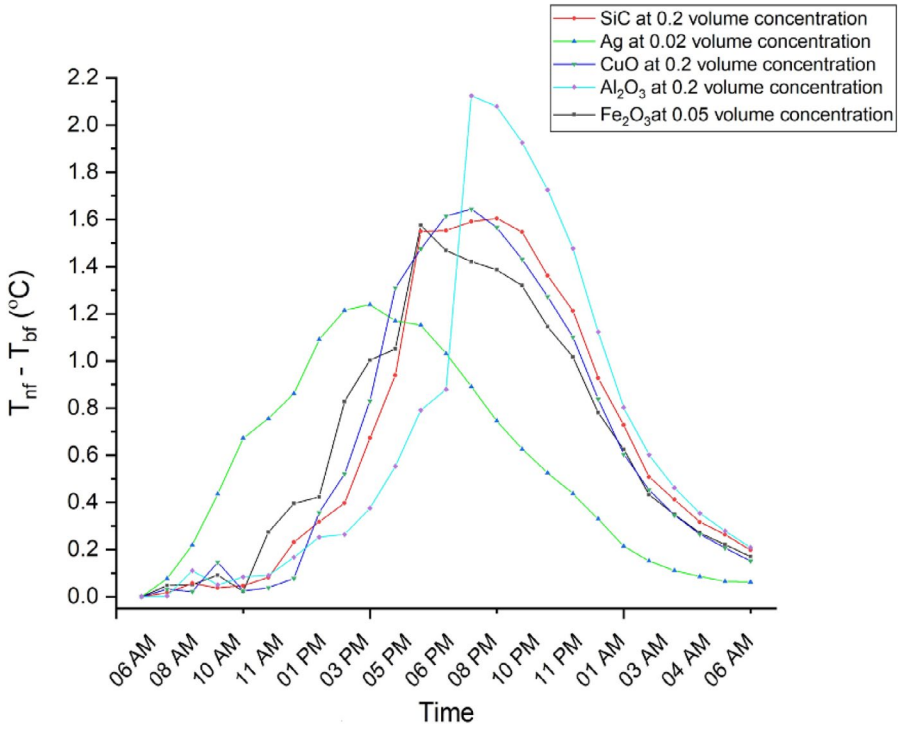

FIGURE 12 Hourly variation of 'ΔT' between base-fluid (water) and different nanofluids

hours because of the resonant nature in near IR and the visible spectrum of nanoparticles. As the temperature of the nanofluid increases, the total heat transfer rate also increases.

6 | CONCLUSIONS

In the present study, the performance of five different nanofluids and base-fluid has been analyzed. On the basis of the present study, the following conclusions are drawn:

1. The optimum water depth for single-slope solar still having water as a base fluid was found to be 2 cm. It has been found that if we increase the basin water depth, the inertia of water increases which leads to a decrease in productivity of still.
2. The peak temperature value during sunshine hours is maximum for Al_2O_3 at a volume concentration of 0.2, followed by CuO. Ag, Fe_2O_3, and SiC.
3. During sunshine hours, the solar absorption for the metallic nanoparticle was found to be maximum because of the resonant nature in near IR and visible spectrum. Thus, resulting in higher water temperatures.
4. Theoretical analysis by temporal discretization show a deviation of around 54% with a time step $\Delta t = 0.1$ sec, but as the value of the time step increases, the temperatures values obtained for the next hour shows an exponential deviation. So, to obtain promising results both space and time should be discretized.
5. The experimental results are in good agreement with theoretical with a total deviation of 12.24% for both experimental and theoretical distillate output for a day and at higher temperatures, the range of deviation was found to be more.

NOMENCLATURE

A	Area of still (m^2)
Cp	Specific heat (J/kgK)
d_p	Diameter of nanoparticle (nm)
F_R	Heat removal factor
h_{cw}	Convective heat transfer coefficient of water (W/m^2°C)
h_{ew}	Evaporative heat transfer coefficient of water (W/m^2°C)
h_{rw}	Radiative heat transfer coefficient between water and glass (W/m^2°C)
h_{cg}	Convective heat coefficient between glass and ambient (W/m^2°C)
h_{rg}	Radiative heat transfer coefficient between glass and sky (W/m^2°C)
h_w	Heat transfer coefficient from basin to water (W/m^2°C)
I(t)	Solar incident radiation on solar still (W/m^2)

I(t)	Solar incident radiation on Collector surface (W/m^2)
K	Thermal conductivity (W/mK)
K_i	Thermal conductivity of insulation (W/mK)
L_i	Thickness of insulation (m)
LH	Latent heat of vaporization (J/kg)
m	Mass of water (kg)
m_{ew}	Mass of evaporated water (kg)
m_d	Hourly mass of distillate produced (kg/m^2hr)
P_g	Partial vapor pressure on glass temperature (Pa)
Pr	Prandtl number = $(\mu_f C_f / K_f)$
P_w	Partial vapor pressure on water temperature (Pa)
Re	Reynolds number = $(\rho VD/\mu)$
$Q_{c,}$	Convective heat transfer (W)
Q_e	Evaporative heat transfer (W)
Q_r	Radiative heat transfer (W)
Q_w	Bottom and side heat transfer losses in the still (W)
Q_u	Heat transfer from solar collector (W)
T_b	Temperature of basin (°C)
U_L	Overall heat transfer coefficient (W/m^2°C)
Φ	Volume fraction
Δt	Time step (sec)

GREEK LETTERS

ε	Emissivity
r	Reflectivity of water
τ	Transmittivity of water
ρ	Density of water (kg/m^3)
μ	Dynamic viscosity of water (Ns/m^2)
β	Inclination angle of glass cover (degree)
α	Fraction of solar energy absorbed
σ	Stefan-Boltzman constant (W/m^2K^4)
β_{nf}	Coefficient of volumetric thermal expansion of nanofluid (K^{-1})
β_v	Coefficient of volumetric thermal expansion of water vapor (K^{-1})
β_{np}	Coefficient of volumetric thermal expansion of nanoparticle (K^{-1})

SUBSCRIPTS AND SUPERSCRIPTS

a	Ambient
b	Basin
bf	Basefluid
c	Convective
e	Evaporative
g	Glass
nf	Nanofluid
r	Radiative
v	Vapor

ORCID

Nima Khalilpoor https://orcid.org/0000-0001-9864-8152

REFERENCES

1. Karagiannis IC, Soldatos PG. Water desalination cost literature: review and assessment. *Desalination*. 2008;223:448-456.
2. Adibi Toosi SS, Goshayeshi HR, Zeinali HS. Experimental investigation of stepped solar still with phase change material and external condenser. *J Energy Storage*. 2021;40:102681.
3. Dwivedi VK, Tiwari GN. Comparison of internal heat transfer coefficients in passive solar stills by different thermal models: An experimental validation. *DES*. 2009;246:304-318.
4. Xiao G, Wang X, Ni M, et al. A review on solar stills for brine desalination. *Appl Energy*. 2013;103:642-652.
5. Tiwari GN, Thomas JM, Khan E. Optimisation of glass cover inclination for maximum yield in a solar still. *Heat Recovery Syst CHP*. 1994;14:447-455.
6. Nafey AS, Abdelkader M, Abdelmotalip A, Mabrouk AA. Enhancement of solar still productivity using floating perforated black plate. *Energy Convers Manage*. 2002;43:937-946.
7. Singh AK, Tiwari GN, Sharma PB, Khan E. Optimization of orientation for higher yield of solar still for a given location. *Energy Convers Manage*. 1995;36(3):175-181.
8. Aboul-Enin S, El-Sebaii AA, El-Bialy E.. Investigation of a single-basin solar still with deep basins. Renew. *Energy*. 1998;14:299-305.
9. Ali Samee M, Mirza UK, Majeed T, Ahmad N. Design and performance of a simple single basin solar still. *Renew Sust Energ Rev*. 2007;11(3):543–549.
10. Abu-Hijleh BAK. Enhanced solar still performance using water film cooling of the glass cover. *Desalination*. 1996;107:235-244.
11. Tiwari AK, Tiwari GN. Thermal modeling based on solar fraction and experimental study of the annual and seasonal performance of a single slope passive solar still: The effect of water depths. *Desalination*. 2007;207:184-204.
12. Dunkle RV. Solar water distillation: the roof type still and a multiple effect diffusion still. *Proc Int Heat Transf Conf Univ Color USA*. 1961;895.
13. Kumar S, Tiwari GN, Singh HN. Annual performance of an active solar distillation system. *Desalination*. 2000;127:79-88.
14. Sakthivel M, Shanmugasundaram S, Alwarsamy T. An experimental study on a regenerative solar still with energy storage medium — Jute cloth. *Desalination*. 2010;264:24-31.
15. Srivastava PK, Agrawal SK. Experimental and theoretical analysis of single sloped basin type solar still consisting of multiple low thermal inertia floating porous absorbers. *Desalination*. 2013;311:198-205.
16. El-bahi A, Inan D. Analysis of a parallel double glass solar still with separate condenser. *Renew Energy*. 1999;17:509-521.
17. Abu-arabi M, Zurigat Y, Al-hinaib H, Al-hiddabib S. Modeling and performance analysis of a solar desalination unit with double-glass cover cooling. *Desalination*. 2002;143:173-182.
18. El-Sebaii AA, Aboul-Enein S, El-bialy E. Single basin solar still with baffle suspended absorber. *Energy Convers Manag*. 2000;41:661-675.
19. Al-Hussaini H, Smith IK. Enhancing of solar still productivity using vacuum technology. *Energy Convers Manag*. 1995;36:1047-1051.
20. Sodha M, Kumar A, Tiwari GN, Tyagi RC. Simple multiple wick solar still: Analysis and performance. *Sol Energy*. 1981;26:127-131.

21. Ramezanizadeh M, Ahmadi M, Nazari M, Sadeghzadeh M, Chen L. A review on the utilized machine learning approaches for modeling the dynamic viscosity of nanofluids. *Renew Sustain Energy Rev*. 2019;114:109345.
22. Sadeghzadeh M, Ahmadi M, Kahani M, Sakhaeinia H, Chaji H, Chen L. Smart modeling by using artificial intelligent techniques on thermal performance of flat - plate solar collector using nanofluid. *Energy Sci Eng*. 2019;7(5):1649-1658.
23. Aghayari R, Maddah H, Pourkiaei SM, Ahmadi MH, Chen L, Ghazvini M. Theoretical and experimental studies of heat transfer in a double-pipe heat exchanger equipped with twisted tape and nanofluid. *Eur Phys J plus* 2020;135(2):1-26.
24. Nasirzadehroshenin F, Sadeghzadeh M, Khadang A, et al. Modeling of heat transfer performance of carbon nanotube nanofluid in a tube with fixed wall temperature by using ANN–GA. *Eur Phys J plus*. 2020;135:217.
25. Mahian O, Kianifar A, Zeinali Heris S, Wongwises S. First and second laws analysis of a minichannel-based solar collector using boehmite alumina nanofluids: Effects of nanoparticle shape and tube materials. *Int J Heat Mass Transf*. 2014;78:1166-1176.
26. Mahian O, Kianifar A, Heris SZ, Wen D, Sahin AZ, Wongwises S. Nanofluids effects on the evaporation rate in a solar still equipped with a heat exchanger. *Nano Energy*. 2017;36:134-155.
27. Chaji H, Ajabshirchi Y, Esmaeilzadeh E, Heris SZ, Hedayatizadeh M. Experimental study on thermal efficiency of flat plate solar collector using TiO2/water nanofluid. *Modern Appl Sci*. 2013;7:60-69.
28. Mahdavi M, Sharifpur M, Meyer JP, Chen L. Thermal analysis of a nanofluid free jet impingement on a rotating disk using volume of fluid in combination with discrete modelling. *Int J Therm Sci*. 2020;158:106532
29. Sahota L, Gupta V, Tiwari G. Analytical study of thermophysical performance of nanofluid loaded hybrid double slope solar still. *J Heat Transfer*. 2018;140:112404.
30. Sahota L, Tiwari GN. ScienceDirect Effect of Al 2 O 3 nanoparticles on the performance of passive double slope solar still. *Sol ENERGY*. 2016;130:260-272.
31. Mahian O, Kianifar A, Kalogirou SA, Pop I, Wongwises S. International Journal of Heat and Mass Transfer A review of the applications of nanofluids in solar energy. *HEAT MASS Transf*. 2013;57:582-594.
32. Omara ZM, Kabeel AE, Essa FA. Effect of using nanofluids and providing vacuum on the yield of corrugated wick solar still. *Energy Convers Manag*. 2015;103:965-972.
33. Sharshir S, Peng G, Wu L, et al. Enhancing the solar still performance using nanofluids and glass cover cooling : Experimental study. *Appl Therm Eng*. 2017;113:684-693.
34. Rashidi S, Bovand M, Rahbar N, Esfahani JA. Steps optimization and productivity enhancement in a nanofluid cascade solar still. *Renew Energy*. 2017;118:536-545.
35. Chen W, Zou C, Li X, Li L. Experimental investigation of SiC nanofluids for solar distillation system: Stability, optical properties and thermal conductivity with saline water- based fluid. *Int J Heat Mass Transf* 2017;107:264-270.
36. Kabeel AE, Omara ZM, Essa FA, Abdullah AS, Arunkumar T. Augmentation of a solar still distillate yield via absorber plate coated with black nanoparticles. *Alexandria Eng J*. 2017;4:433-438.
37. Liu X, Xuan Y. Full-spectrum volumetric solar thermal conversion via photonic nanofluids. *Nanoscale*. 2017;9(39):14854-14860
38. Shadi M, Abujazar S, Fatihah S, Kabeel AE. Seawater desalination using inclined stepped solar still with copper trays in a wet tropical climate. *Desalination*. 2017;423:141-148.
39. Elashmawy M. An experimental investigation of a parabolic concentrator solar tracking system integrated with a tubular solar still. *Desalination*. 2017;411:1-8.
40. Sahota L, Tiwari GN. Effect of nano fl uids on the performance of passive double slope solar still : A comparative study using characteristic curve. *DES*. 2016;388:9-21.
41. Kabeel AE, Sathyamurthy R, Manokar AM, Sharshir SW, Essa FA, Elshiekh AH. Experimental study on tubular solar still using Graphene Oxide Nano particles in Phase Change Material (NPCM ' s) for fresh water production. *J Energy Storage*. 2020;28:101204
42. Subhedar DG, Chauhan KV, Patel K, Ramani BM. Performance improvement of a conventional single slope single basin passive solar still by integrating with nanofluid-based parabolic trough collector : An experimental study. *Mater Today Proc*. 2020;26:1478-1481.

How to cite this article: Dhindsa GS, Kumar V, Mittal MK, et al. Performance Comparison of single-slope solar still loaded with various nanofluids. *Energy Sci Eng*. 2021;00:1–14. https://doi.org/10.1002/ese3.993

APPENDIX

TABLE A11 Thermo Physical properties of water vapor

Density	ρ_v	$353.44/(T_v + 237.15)$
Specific heat	C_v	$999.2 + 0.1434T_v + 1.101T_v^2 - 6.7581 \times 10^{-8} T_v^3$
Viscosity	μ_v	$1.718 \times 10^{-5} + 4.620 \times 10^{-8} T_v$
Thermal Conductivity	K_v	$00244 + 0.7673 \times 10^{-4} T_v$
Thermal expansion coefficient	β_v	$1/(T_v + 273.15)$
Properties of water:		
Density	ρ_w	$1000\left[1 - (T_w - 4)^2/\left(119000 + 1365T_w\right) 4T_w^2\right]$
Specific heat	C_w	$4217.629 - 3.20888T_w + 0.09503T_w^2 - 0.00132T_w^3 + 9.415 \times 10^{-6} T_w^4 - 2.5479 \times 10^{-8} T_w^5$
Viscosity	μ_w	$0.00169 - 4.25263 \times 10^{-5} T_w + 4.9255 \times 10^{-7} T_w^2 - 2.0993504 \times 10^{-9} T_w^3$
Thermal Conductivity	K_w	$0.56112 + 0.00193T_w - 2.60152749 \times 10^{-6} T_w^2 - 6.08803 \times 10^{-8} T_w^3$

TABLE A12 Thermo Physical properties of Nanofluid

Density	ρ_{nf}	$\rho_{nf} = \left(1 - \varnothing_p\right) \rho_{bf} + \varnothing_p \rho_p$
Specific heat	C_{nf}	$C_{nf} = \left[\left(1 - \varnothing_p\right) \rho_{bf} C_{bf} + \varnothing_p \rho_p C_p\right] / \rho_{nf}$
Viscosity	μ_{nf}	$\left[\left(1+\varnothing_p\right)^{11.3} \left(1+\frac{T_{nf}}{70}\right)^{-0.038} \left(1+\frac{d_p}{170}\right)^{-0.061}\right] \mu_{bf}$
Thermal Conductivity	K_{nf}	$K_{eff} = \left[1 + 4.4\left(\mathrm{Re}^{0.4} Pr^{0.66}\right)\left(\left(T_{nf}/T_{fr}\right)^{10} \left(K_p/K_{bf}\right)^{0.03} \varnothing_p^{0.66}\right)\right] K_{bf}$
Thermal expansion coefficient	β_{nf}	$\beta_{nf} = \left(1 - \varnothing_P\right) \beta_{bf} + \varnothing_P \beta_{np}$